

On hysteresis and air gap disturbance in current and voltage mode feed-forward control of variable reluctance actuators

A. Katalenic, C.M.M. van Lierop and P.P.J. van den Bosch

Abstract—Current and voltage mode control approaches in feed-forward force control of variable reluctance actuators are analyzed and compared. Two major error generators, the unknown air gap variation and hysteresis, are investigated together with the quantification of their influence on the final force tracking error, and it is shown that voltage control has fundamental advantages over current control. Furthermore, linearization laws with hysteresis compensation based on the parametric hysteresis operator are proposed and compared on a high-fidelity actuator model which is derived from the behavior of magnetic materials, the actuator structure, and first principle physical models.

I. INTRODUCTION

Due to constant demand for faster production in industrial mechatronical systems, e.g. semi-conductor industry, higher accelerations and thus higher forces and less mass is required from the force actuators. The actuator concept based on permanent magnets and Lorentz forces acting on a conducting coil, i.e. a voice coil actuator, has reached its peak with respect to performance criteria like maximum force and power dissipation per unit volume [1], which means that the further increase of the required force output comes at the cost of increased mass and power dissipation, which requires additional cooling and additional mass. For that reason, other actuator architectures have to be explored. An interesting concept in electromagnetism are so-called magnetic circuits in which closed loops of magnetic field lines are analyzed as circuits of magnetic flux flowing through ferromagnetic materials. When such circuits include moving parts, a reluctance force source controllable by the excitation coil current is obtained [2]. The reluctance force is usually proportional with the square of the excitation current. When compared to the linear current to force relationship of the voice coil actuators, it brings obvious advantages in the maximal obtainable force to current ratios. Also, most reluctance force based topologies eliminate the need for permanent magnets, which has economical advantages, e.g. price, and eliminates the effects of demagnetization. On the other hand, the purely attractive nature of the reluctance force, input to output non-linearity, high negative position stiffness and parasitic magnetic effects like hysteresis, eddy currents, leakage and fringing put limitations on the controllability and the reproducibility of such actuators [3]. Regardless of that, the variable reluctance concept has been, among other, successfully applied in rotary machines [4] and active

magnetic bearings [3]. There are many available control solutions which deal with controllability issues [7], input output non-linearity [5],[6],[15], [17], losses minimization [8] and the lack of sensors [9].

In high-precision positioning applications, as discussed in [10], feed-forward control plays an important role since it doesn't share the low-gain margin problem of the feedback approach and can therefore give rise to substantial improvements in the positioning precision at high frequencies, even in presence of model uncertainties [11]. This paper deals with modeling and feed-forward control, i.e. linearization of variable reluctance force actuators for a new potential application area in high-precision and high-bandwidth motion control. The main focus is put on the negative position stiffness, i.e. high sensitivity of the actuator model to the unknown air gap variation and hysteresis in the force, which are usually neglected [5], [15], [17] because of their small amplitude. However, they cause performance degradation in nanometer positioning applications [13]. The effects of these disturbances on the force error are quantified for current-mode and voltage-mode feed-forward control of reluctance actuators, and it is shown that voltage-mode control has fundamental advantages. A parametric hysteresis inverse [20], which was used to invert hysteresis in current-mode operated reluctance force actuators [21], is used for the analysis and synthesis of the voltage-mode hysteresis compensation law. Simulation results are demonstrated on a high-fidelity actuator model which is derived from fundamental physical laws and magnetization laws of materials.

II. ACTUATOR MODEL WITH HYSTERESIS

When modeling the behavior of variable reluctance actuators, the magnetization of magnetic cores is usually approximated by a linear $B = \mu_0 \mu_r H$ law and very often neglected since it is dominated by the air gap [18]. The obtained force model with neglected magnetization effects is still non-linear and shows various effects problematic and challenging for control design. In this paper, in order to obtain a more realistic model of the reluctance force actuator with respect to magnetization effects of the core, fundamental physical laws together with general models and observations for magnetization of ferromagnetic materials formulated in [12] and [16] are used. Generally, the behavior of the reluctance force actuator can be split into three domains: the electrical domain which includes the electric excitation circuit, the magnetic domain which includes the magnetic core and the surrounding air where the magnetic field is formed, and the mechanical domain which includes the detached core part, i.e. the floater which is free to move under the influence of

This research is being conducted within the *Pieken in de Delta* program of the Dutch Ministry of Economic Affairs. A. Katalenic, C.M.M. van Lierop and P.P.J. van den Bosch are with Department of Electrical Engineering, Eindhoven University of Technology, P.O. Box 513, 5600 MB Eindhoven, The Netherlands, E-mail: a.katalenic@tue.nl

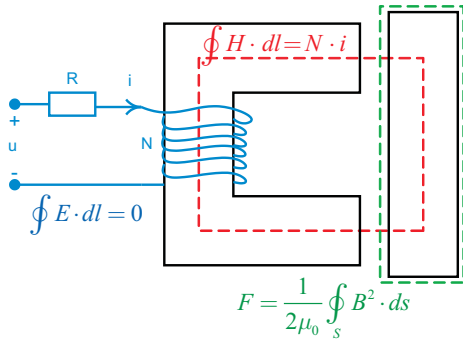


Fig. 1. Schematics of a C-core linear variable reluctance actuator with the corresponding scalar physical laws that describe its behavior.

the attractive reluctance force. This separation is depicted in Fig. 1 together with the corresponding fundamental laws governing the actuator's behavior. It has to be noted that all quantities are assumed lumped.

The electric circuit is described by *Kirchhoff's voltage law*, and *Faraday's law of induction*:

$$u = R \cdot i + NA \cdot \frac{dB}{dt}, \quad (1)$$

where u denotes the input voltage, R the excitation coil resistance, N the total number of coil turns, A is the assumed constant cross-sectional area of the actuator, and B is the magnetic flux density which is assumed equally distributed.

The *Ampere's circuital law*, and the field separation principle from [12] yields:

$$N \cdot i = \frac{2g}{\mu_0} \cdot B + (H_h + H_{clas} + H_{exc}) \cdot l_m, \quad (2)$$

where H_h denotes the hysteresis field, H_{clas} the classical eddy-current field, H_{exc} the excess field, B the magnetic flux density, g the air gap size, and l_m the mean magnetic circuit length. The attractive force on the floater follows from the *Maxwell's stress tensor* and is given by [18]:

$$F = \frac{A}{\mu_0} B^2. \quad (3)$$

An approximate lumped model for the eddy current field and excess field in the core material is obtained from [12]:

$$H_{clas} = \frac{\sigma d^2}{12} \frac{dB}{dt}, \quad (4)$$

where σ is the material electrical conductivity and d is the lamination thickness, and:

$$H_{exc} = \delta \sqrt{\sigma G S V_0} \left| \frac{dB}{dt} \right|^{\frac{1}{2}}, \quad (5)$$

where $\delta = \text{sgn}\left(\frac{dB}{dt}\right)$, $G = 0.1356$ is a dimensionless coefficient, $S = d\sqrt{A}$ is the lamination cross-sectional area, and V_0 is an experimentally fitted parameter. The hysteresis field $H_h(B)$ can be calculated (approximated) by any inverse ferromagnetic hysteresis model. In this paper, the inverse model proposed in [14] together with the corresponding

values for Permalloy is used. From (1), (2), (4), and (5), the following relation is obtained:

$$\underbrace{\left(\frac{l_m \sigma d^2}{12} + \frac{NA^2}{R} \right)}_a \frac{dB}{dt} + \underbrace{\delta \sqrt{\sigma G S V_0}}_b \left| \frac{dB}{dt} \right|^{\frac{1}{2}} = \underbrace{\frac{N}{R} u - H_h(B) - \frac{2g}{\mu_0} B}_{c(u,B)}, \quad (6)$$

which can be solved for $\frac{dB}{dt}$ to obtain:

$$\frac{dB}{dt} = \frac{\text{sgn}[c(u,B)]}{4} \left(\sqrt{\left(\frac{b}{a} \right)^2 + \frac{4}{a} |c(u,B)|} - \frac{b}{a} \right)^2. \quad (7)$$

The variable reluctance actuator model used for simulation purposes is then given by (3), (6), (7), together with $H_h(B)$ calculated with the inverse hysteresis model of choice, in our case [14].

Remark II.1 Compared to other approaches where a hysteresis model is fitted to the total bulk behavior of the system [13],[19], in this article the final hysteretic behavior of the reluctance force actuator is constructed from the material properties and the actuator structure. The benefit of this approach is the possibility to extend a large available research on magnetic field effects in the magnetic materials to the specific case of the variable reluctance actuator without a need to develop a new framework. Moreover, this model gives more physical insight when compared to only input-output modeling approaches.

Remark II.2 Although the proposed reluctance actuator model was not yet verified on an experimental setup, it is expected that the physical actuator will show similar effects, since the model was derived from fundamental physical laws and empirical models derived by distinctive authors. Moreover, in the modeling process, the emphasis was put on the reproducibility of the hysteresis in the force and the general behavior with respect to air gap variations, so other parasitic effects such as leakage flux and fringing were neglected.

III. INVERSE MODELS WITH THE PARAMETRIC HYSTERESIS OPERATOR

A. Parametric hysteresis operator

Control synthesis requires simple models of phenomena that are still sufficiently accurate, directly implementable, easily identifiable, and mathematically well defined. For the purpose of hysteresis compensation in the variable reluctance actuators, a parametric direct and inverse hysteresis operator pair is used in this paper. This operator is formally defined and analyzed in [20], whereas the identification procedure and hysteresis compensation results for current-mode variable reluctance actuator are given in [21], where an order of magnitude improved compensation compared to the best single-valued compensation was experimentally verified. This operator will be used in the analysis present in this

paper, since it can be mathematically manipulated, is directly implementable in a digital controller, and gives a very good approximation of hysteretic effects for synthesis of control laws for variable reluctance actuators.

Definition III.1 Let $v(t), u_d(t) \in C^\infty$, $k_1, k_2 \in \mathbb{R}^+$. Then the *inverse parametric hysteresis operator* :

$$v(t) = H^{-1}(k_1, k_2) [u_d(t)] \quad (8)$$

is defined as:

$$\tilde{v}(t) = \tilde{u}(t) + M \cdot \left(1 - e^{-k_2 \tilde{u}(t)}\right) \quad (9)$$

where $\tilde{u}(t) = |u(t) - u_0|$, $\tilde{v}(t) = |v(t) - v_0|$, $M = (u_0 - v_0) \operatorname{sgn} \dot{u} + k_1$, and $u_0 = u(\tau^*)$ and $v_0 = v(\tau^*)$ where:

$$\tau^* = \begin{cases} \sup_{\dot{u}(\tau)=0, \ddot{u}(\tau) \neq 0, \tau \leq t} \tau & \text{for } t > 0 \\ 0 & \text{for } t = 0, \end{cases}$$

i.e. τ^* is the last time instant at which $\dot{u}(t)$ changed sign. Furthermore, the operator H^{-1} has memory since u_0 and v_0 are stored.

The operator basically defines an exponential convergence with rate k_2 from the point (u_0, v_0) towards the affine asymptotes defined by k_1 . The left and the right inverse of (8), i.e. the direct hysteresis operator, can be constructed using the *Lambert W* function. For the definition of the direct hysteresis operator and more properties of the inverse operator, the reader is referred to [20].

B. Inverse compensation

For feed-forward linearizing control, inverse models of the reluctance force actuator have to be constructed. Rate-dependent terms in (2) will be neglected since their influence is negligible in thin core material laminations within the operating bandwidth.

After neglecting the rate-dependent terms in (2) the following is obtained: $N \cdot i = \frac{2g}{\mu_0} \cdot B + H(B) \cdot l_m$, where $H(\cdot)$ is the parametric hysteresis operator. Further we can write:

$$\begin{aligned} i &= \frac{2g}{\mu_0 N} \cdot B + \frac{l_m}{N} \cdot \tilde{B} + \frac{l_m}{N} M \left(1 - e^{-k_2 \tilde{B}}\right) \\ &\approx f(g, B) + \frac{l_m M}{N} \left(1 - e^{-k_2^* \cdot f(g, B)}\right) \\ &\approx H^{-1}(k_1^*, k_2^*) [f(g, B)] \end{aligned} \quad (10)$$

where $f(g, B) = \frac{2g}{\mu_0 N} \cdot B$ is a single-valued model of the magnetic circuit which can be represented in other ways, e.g. with polynomials [6] or 2D spline [21] to include all other effects, like flux leakage, which were neglected in our analysis. H^{-1} is the inverse parametric hysteresis operator (8). The parameters k_1^* and k_2^* can be determined by geometrical fitting of the input-output map of the operator to the measurements and possible further optimization in order to obtain a better fit [21]. The function $f(g, B)$ can be identified separately from H^{-1} [21].

The linearizing law (10), i.e. a practical implementation of the described parametric hysteresis inverse, was experimentally verified in [21], where it was shown that the error due

to hysteresis was reduced by order of magnitude for different air gap sizes.

In the case of voltage control, the feed-forward compensation law is obtained from (1) and (10):

$$u_{FF} = R \cdot i_{FF} + NA \cdot \frac{dB_d}{dt}. \quad (11)$$

The voltage-mode linearizing law is load resistance dependent, which means that the current information is still necessary to estimate the resistance change in (11). Furthermore, the desired magnetic field densities B_d in (10), (11), (12) and (13) are obtained from the desired force profile by using the inverse of (3).

Remark III.2 Current and voltage mode linearizing laws (10) and (11) without hysteresis compensation will be used in the analysis and are given by:

$$i_{FF}^* = \frac{2g}{\mu_0 N} \cdot B_d, \quad (12)$$

$$u_{FF}^* = R \cdot i_{FF}^* + NA \cdot \frac{dB_d}{dt}, \quad (13)$$

IV. FEED-FORWARD CONTROL ERROR ANALYSIS

A. Air gap variation

As it will be shown, the force of the C-core reluctance force actuator is highly air gap dependent, which results in large errors of inverse models for feed-forward control in case the air gap is not accurately known. The analysis and quantification of this error will be carried out by assuming no hysteresis in the actuator, i.e. the core magnetic field components H_h , H_{clas} and H_{exc} in (2) will be neglected.

In case of the current-mode control, after applying the linearizing law (12), we get: $\frac{2g}{\mu_0} \cdot B - \frac{2g^*}{\mu_0} B_d = 0$.

If a mismatch between the real air gap g and the estimated one g^* , denoted with $\Delta g = g - g^*$ is assumed, we get:

$$\frac{\Delta B}{\Delta g} = -\frac{B_d}{g^*}, \quad (14)$$

where $\Delta B = B - B_d$ is the final error in the obtained magnetic flux density.

In case of voltage-mode control, after applying the linearizing law (13), the following is obtained: $\frac{2Rg^*}{\mu_0 N} \cdot B_d - \frac{2Rg}{\mu_0 N} \cdot B + NA \frac{dB_d}{dt} - NA \frac{dB}{dt} = 0$.

With $\Delta g = g - g^*$ and $\Delta B = B - B_d$, it becomes: $\frac{2Rg}{\mu_0 N} \Delta B + NA \frac{d\Delta B}{dt} = -\frac{2R\Delta g}{\mu_0 N} B_d$.

Since, in this section, the effects of Δg on ΔB are of interest, B_d and g^* are assumed constant, which yields an linear differential equation. This equation, after applying the *Laplace transformation*, becomes:

$$\frac{\Delta B(s)}{\Delta g(s)} = -\frac{B_d}{g^*} \cdot \frac{1}{1 + s \cdot T_{\Delta g}}, \quad (15)$$

where $T_{\Delta g} = \frac{\mu_0 N^2 A}{2Rg}$.

When comparing (14) and (15) it can be seen that the influence of the air gap variation on the final error in the magnetic field is damped with time constant $T_{\Delta g}$ in case of voltage-mode control. These results are formalized for the force error in the following proposition:

Proposition IV.1 In case the core magnetic field contributions in (2) are neglected, and the non-measured position disturbance Δg is given by $\Delta g = A_g \cdot \sin(\omega_g t)$, then the bound on the output force disturbance in case of current-mode linearization (12) is given by:

$$|\Delta F| \lesssim \frac{3F_d}{g^{*2}} A_g^2 + \frac{2F_d}{g^*} A_g. \quad (16)$$

On the other hand, the bound on the output force disturbance in case of voltage-mode linearization (13) is given by:

$$|\Delta F| \lesssim \frac{3F_d}{g^{*2}} S(\omega_g)^2 A_g^2 + \frac{2F_d}{g^*} S(\omega_g) A_g, \quad (17)$$

where $T_{\Delta g} = \frac{\mu_0 N^2 A}{2Rg}$ and $S(\omega) = \frac{1}{\sqrt{1+\omega^2 T_{\Delta g}^2}}$ is an air gap disturbance frequency dependent scaling.

Proof: From (3) we obtain: $\Delta F = 2\sqrt{\frac{A}{\mu_0}} F \cdot \Delta B$, which together with (14) and by writing $F = F_d - \Delta F$ gives: $\Delta F = -2\sqrt{F_d} \sqrt{F_d - \Delta F} \cdot \frac{\Delta g}{g^*}$. Solving it for ΔF gives the following second-order approximation:

$$\begin{aligned} \Delta F &= -2F_d \left(\frac{\Delta g}{g^*} \right)^2 - 2F_d \sqrt{\left(\frac{\Delta g}{g^*} \right)^2 + 1} \cdot \frac{\Delta g}{g^*} \\ &\approx -2F_d \left[\frac{3}{2} \left(\frac{\Delta g}{g^*} \right)^2 + \frac{\Delta g}{g^*} \right] = -\frac{3F_d}{g^{*2}} \Delta g^2 - \frac{2F_d}{g^*} \Delta g. \end{aligned} \quad (18)$$

The expression (16) is then obtained using the bias and first harmonic approximation (i.e. describing function) of (18).

In case of voltage-mode control, the expression (17) can be written as $\frac{\Delta B(s)}{\Delta g_V(s)} = \frac{B_d}{g^*}$ where $\Delta g_V(s) = \Delta g(s) \cdot \frac{1}{1+sT_{\Delta g}}$. We can therefore assume the new attenuated disturbance $\Delta g_V = S(\omega_g) \Delta g$, where $S(\omega_g) = \frac{1}{\sqrt{1+\omega_g^2 T_{\Delta g}^2}}$ and replace Δg in (18) to obtain (17) after bias and first order harmonic approximation. ■

Remark IV.2 In case of voltage-mode control, the air gap disturbance is damped with the time constant $T_{\Delta g}$ when compared to current-mode control, i.e. voltage-mode control preserves the intrinsic damping of the actuator. Furthermore, it is important to observe that $S(\omega) < 1$, i.e. the position disturbance will always be more damped in case of voltage-mode control. Also, $S(\omega_g \rightarrow 0) \rightarrow 1$, meaning the steady-state behavior of both schemes will be the same, i.e. the difference is visible only during transients.

It can be concluded that the current source adds undesired negative force position stiffness, since it counteracts any back EMF induced by the air-gap variation. A voltage source, on the other hand, permits current change due to back EMF and, therefore, keeps the intrinsic damping mechanism in place.

B. Hysteresis

In this subsection the force error due to neglected hysteresis present in the system is analyzed together with the comparison of voltage-mode and current-mode control. Similar analysis applies when the hysteresis is partially compensated. If rate dependent damping fields in (2) are neglected, the current-mode feed-forward control law (12)

gives the following relation: $\frac{2g^*}{\mu_0} \cdot B_d = \frac{2g}{\mu_0} \cdot B + H_h(B) \cdot l_m$. The hysteresis term $H_h(\tilde{B})$ can be approximated with the parametric inverse hysteresis operator (8): $H_h(B) = \frac{1}{\mu_0 \mu_r} H^{-1}(\mu_0 \mu_r H_c, k_2)[B]$, where $\mu_0 \mu_r$ is the slope of the anhysteretic curve, i.e. the effective slope of the hysteresis loop and H_c is the coercitive field, i.e. the effective width of the hysteresis loop of the core material, and k_2 is the parameter defining the smoothness of the transitions inside the major loop.

With current-mode linearizing control (12), $g^* = g$ and $\Delta B = B - B_d$, the following is obtained:

$$\begin{aligned} \frac{2g}{\mu_0} B_d &= \frac{2g}{\mu_0} B + \frac{l_m}{\mu_0 \mu_r} \tilde{B} + l_m H_c \left(1 - e^{-k_2 \tilde{B}}\right) \\ \Delta B &\approx \frac{\mu_0 l_m H_c}{2g} \left(1 - e^{-k_2 \tilde{B}}\right) = \frac{\mu_0 l_m H_c}{2g} \cdot S_H(\tilde{B}), \end{aligned} \quad (19)$$

where $S_H(\tilde{B}) = \left(1 - e^{-k_2 \tilde{B}}\right) < 1$ is the magnetic field amplitude dependent scaling of the hysteresis error.

For sinusoidal inputs $B_d = B_{dm} \sin(\omega t)$ and after using the identity $\max(\tilde{B}) = 2B_{dm}$, which can be shown to hold for periodic inputs from the definition III.1, the relation (19) becomes:

$$|\Delta B_I| \lesssim \mu_0 H_c \cdot \frac{l_m}{2g} \cdot S_H(2B_{dm}). \quad (20)$$

The equation (20) shows that the error due to hysteresis is scaled with $\frac{l_m}{2g}$ which depends on the actuator structure, and S_H which depends on the amplitude of the desired field signal.

On the other hand, the voltage-mode linearizing control (13) yields: $\frac{2g}{\mu_0} \Delta B + \frac{N^2 A}{R} \frac{d\Delta B}{dt} = l_m H_c \cdot S_H(\tilde{B})$. For sinusoidal inputs: $B_d = B_{dm} \sin(\omega t)$ it becomes: $\Delta B + \frac{\mu_0 N^2 A}{2Rg} \frac{d\Delta B}{dt} \approx \frac{\mu_0 l_m H_c}{2g} \cdot S_H(2B_{dm})$. Finally, since the hysteresis error will be periodic with the same period as the desired field signal, the following is obtained:

$$|\Delta B_V| \lesssim \mu_0 H_c \cdot \frac{l_m}{2g} \cdot S_H(2B_{dm}) \cdot S(\omega) = S(\omega) \cdot |\Delta B_I|, \quad (21)$$

where ΔB_I is given by (20), $T_H = \frac{\mu_0 N^2 A}{2Rg}$, and $S(\omega) = \frac{1}{\sqrt{1+\omega^2 T_H^2}}$ is a scaling dependent on the field signal frequency.

Remark IV.3 Error expressions (20) and (21) also hold for biased sinusoidal inputs, $B_d = B_0 + B_{dm} \cos(\omega t)$, since \tilde{B} is independent of B_0 for periodic inputs. This can be seen from the definition III.1.

These results are formalized for the force error in the following proposition:

Proposition IV.4 In case the rate-dependent field contributions in (2) are neglected, there is no unknown variation in the air gap g , and the desired force profile is assumed a biased sinusoid $F_d = F_{dm} (1 + \sin(\omega t))$, then an approximative bound on the output force error due to the uncompensated hysteresis, in case of current-mode linearization (12), is given by:

$$|\Delta F_I| \lesssim \mu_0 H_c \cdot S_L S_H(F_{dm}) \sqrt{F_d}. \quad (22)$$

On the other hand, an approximative bound on the output force error in case of voltage-mode linearization (13) is given by:

$$|\Delta F_V| \lesssim \mu_0 H_c \cdot S_L S_H(F_{dm}) S(\omega) \sqrt{F_d}, \quad (23)$$

where $S_L = \sqrt{\frac{A}{\mu_0} \frac{l_m}{g}}$ is an actuator layout dependent scaling of the hysteresis, $S_H = S_H(F_{dm}) = \left(1 - e^{-k_2 \sqrt{\frac{2\mu_0 F_{dm}}{A}}}\right) < 1$ is a field amplitude dependent scaling of the hysteresis and $S(\omega) = \frac{1}{\sqrt{1+\omega^2 \cdot T_H^2}} < 1$ with $T_H = \frac{\mu_0 N^2 A}{2Rg}$ is a desired force signal frequency dependent scaling.

Proof: After inserting (3) and $\Delta F = 2\sqrt{\frac{A}{\mu_0}} F \cdot \Delta B$ into (20), the following is obtained: $\Delta F \lesssim \mu_0 H_c S_L \sqrt{F_d + \Delta F} \cdot S_H(F_m)$. Solving for ΔF yields: $\Delta F \lesssim \frac{(\mu_0 H_c S_L S_H)^2}{2} + \mu_0 H_c S_L S_H \sqrt{F_d} \sqrt{\frac{(\mu_0 H_c S_L S_H)^2}{4F_d} + 1}$. Expression (22) is then obtained after assuming $\mu_0 H_c S_L S_H \ll 2\sqrt{F_d}$. Furthermore, the expression (23) is obtained from (21) and (22) by using the fact that the frequency of the first harmonic of the magnetic field signal will be the same as the frequency of the desired force signal. ■

Remark IV.5 In the expressions (17) and (23) only the amplitude attenuation is considered, while there are also phase shifts in the error due to the intrinsic damping and hysteresis. The analysis of these phase shifts is out of scope of this paper. Furthermore, sinusoidal reference signals and sinusoidal first harmonic approximations were assumed for the convenience of the error expression derivation, as the basic mechanism is valid for general inputs.

Remark IV.6 It can be observed that $T_H = T_{\Delta g}$, i.e. the intrinsic mechanism damping the air gap disturbance is the same as the mechanism damping the hysteresis. Also, both time constants are dependent on the resistance in the electric circuit which includes the excitation coil resistance and the voltage source resistance. The smaller the total resistance, more intrinsic damping there is, and if no resistance and no other losses are assumed, there would be no error due to air gap variation or hysteresis.

V. DEMONSTRATION EXAMPLES

The following numerical parameter values are used for demonstration purposes: $R = 0.8$, $N = 600$, $A = 1 \cdot 10^{-4}$, $g_{nom} = 1 \cdot 10^{-3}$, $l_m = 2 \cdot 10^{-1}$, $\sigma = 2.5 \cdot 10^6$, $d = 1 \cdot 10^{-4}$, $V_0 = 0.1$. These values are chosen so that the actuator produces a force of 250 at the magnetic flux density in the material of 1.8. The material properties were obtained from [12] and the magnetic core hysteresis is simulated by the model [14] with parameters $H_c = 62$, $B_r = 1.7$, $H_{cl} = 400$ and $B_{cl} = 2.1$. H_{cl} and B_{cl} are the field values where the hysteresis loop of the model collapses into a single-valued map.

Three times differentiable trajectories as depicted in Fig. 3 are used as force reference signals. A current-mode linearizing law (12) is used on the model (7) and the air

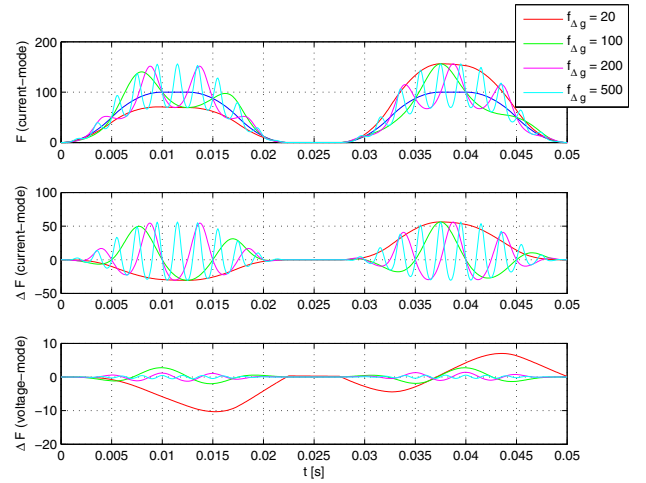


Fig. 2. Force error due to the unmeasured air gap variation for current-mode and voltage-mode feedforward

gap disturbance in the actuator model was set to $\Delta g = 2 \cdot 10^{-4} \cdot \sin(2\pi f_{\Delta g} \cdot t)$. The results are depicted in Fig. 2 where a large force error, independent of the disturbance frequency content, is observable. This observations are in accordance with the expression (16) which gives $-28 \leq \Delta F \leq 52$. The same simulation is repeated with the voltage-mode linearizing law (13) and the results are depicted in Fig. 2 as well. It can be observed that the amplitude of the force error reduces with the frequency of the air gap disturbance. This is in accordance with (17) which gives $-11 \leq \Delta F \leq 13$ in case $f_{\Delta g} = 20$. The error due to non-compensated hysteresis is still present in the results from Fig. 2, but is negligible when compared to the error induced by the air gap disturbance.

On the other hand, in the results depicted in Fig. 3, there is no air gap disturbance, so the error due to the non-compensated hysteresis can be analyzed. It can be observed that, in case of current-mode control, the error in the force is independent of the frequency content of the reference signal. The amplitude of this error is in accordance with (22) which gives $\Delta F \lesssim 3.5$. The same figure shows that the force error in the case of voltage-mode feed-forward control is attenuated with the frequency content of the desired force signal. This is in accordance with the expression (23) which contains an additional scaling factor $S(\omega)$. The force reference signal in Fig. 3 with $dF/dt_{max} = 10000$ has a period of 0.05 s and can therefore be approximated by a biased sinusoidal with frequency $f = 20$. For such a signal, $S(\omega) = 0.12$, yielding $|F_V| \lesssim 0.42$. This is somewhat smaller than the maximal value depicted in Fig. 3, but that is to be expected since first harmonic approximations were used in the derivation of (23).

A comparison of feed-forward laws (10) and (11) based on the parametric hysteresis inverse made on the model (7) is depicted in Fig. 4. It can be seen that the hysteresis inverse significantly improves overall accuracy of the feed-forward laws. Furthermore, the hysteresis compensation error is further damped in case of voltage-mode control. Moreover, the last graph in Fig. 4 shows that the voltage-mode control

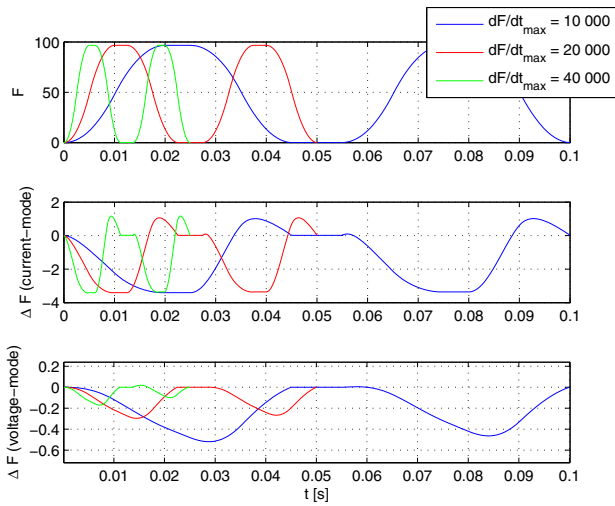


Fig. 3. Force error due to the uncompensated hysteresis.

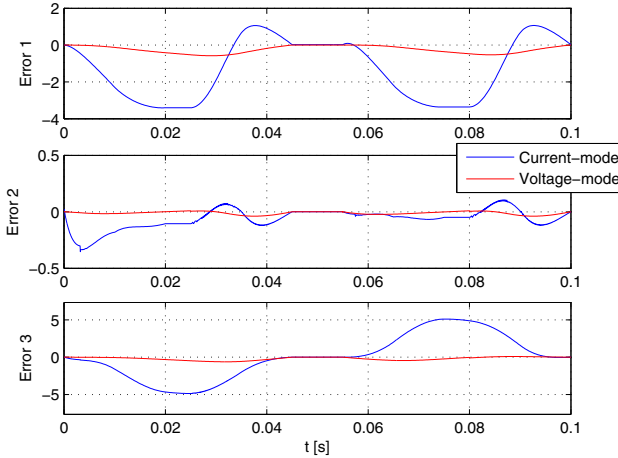


Fig. 4. Comparison of the force error in current-mode and voltage-mode feed-forward control laws. Error1 - no hysteresis compensation present; Error2 - with hysteresis compensation based on the parametric hysteresis inverse; Error3 - with hysteresis compensation and additional air gap disturbance $\Delta g = 1 \cdot 10^{-5} \sin(40\pi \cdot t)$. The desired force profile is as in Fig. 2 or 3.

law (11) outperforms the current-mode control law (10) when both hysteresis and the air gap disturbance are present in the plant.

VI. CONCLUSIONS

In this article, current-mode and voltage-mode feed-forward controllers for variable reluctance actuators were compared on a high-fidelity model. The dependence of the output force error on the actuator structure, magnetic material properties and the working point was quantified for periodic air gap and hysteresis disturbances, for both current and voltage mode control. It was shown that the voltage-mode control has fundamental advantages when compared to the current-mode control, since the unknown high-frequent air gap and hysteresis disturbances are damped by the intrinsic actuator mechanism based on the back EMF. A current source, on the other hand, automatically counteracts this damping, which is especially problematic outside the force control bandwidth,

since those disturbances can no longer be actively damped by the feed-back. The behavior of the current and voltage mode control in presence of low-frequent, quasi-static disturbances was shown to be similar.

Furthermore, the parametric hysteresis inverse was shown to further reduce the force tracking error. This motivates the usage of voltage-mode feed-forward control with hysteresis compensation in high-precision force control of variable reluctance actuators, also in combination with feed-back control. Simulation results illustrate the analysis.

REFERENCES

- [1] N.H. Vrijsen, J.W. Jansen and E.A. Lomonova, "Comparison of linear voice coil and reluctance actuators for high-precision applications," *14th International Power Electronics and Motion Control Conference (EPE/PEMC)*, September 2010.
- [2] J.R. Brauer, "Magnetic Actuators and Sensors," *John Wiley & Sons*, New Jersey, 2006.
- [3] G. Schweitzer and E.H. Maslen, "Magnetic bearings," *Springer-Verlag Berlin Heidelberg*, 2009.
- [4] M. Nashiki, "Switched reluctance motor," U.S. patent no. 6,081,083, Jun. 27, 2000.
- [5] J.D. Lindlau and C.R. Knospe, "Feedback linearization of an active magnetic bearing with voltage control," *IEEE Transactions on Control Systems Technology*, vol. 10, no. 1, pp. 21-31, January 2002.
- [6] M. Chen, C.R. Knospe, "Feedback linearization of active magnetic bearings: Current-mode implementation," *IEEE Transactions on Mechatronics*, vol. 10, no. 6, pp. 632-639, December 2005.
- [7] P. Tsiotras, M. Arcak, "Low-bias control of AMB subject to voltage saturation: state-feedback and observer designs," *IEEE Trans. Contr. Syst. Technol.*, vol. 13, no. 2, pp. 262-273, March 2005.
- [8] T. Hu, Z. Lin, P.E. Allaire, "Reducing power loss in magnetic bearings by optimizing current allocation," *IEEE Trans. Magn.*, vol. 40, no. 3, pp. 1625-1635, May 2004.
- [9] D. Vischer, "Self-sensing active magnetic levitation," *IEEE Trans. Magn.*, vol. 29, no. 2, pp. 1276-1281, March 1993.
- [10] S. Devasia, E. Eleftheriou, and S.O.R. Moheimani, "A survey of control issues in nanopositioning," *IEEE Trans. Contr. Syst. Technol.*, vol. 15, no. 5, pp. 802-823, September 2007.
- [11] S. Devasia, "Should model-based inverse inputs be used as feedforward under plant uncertainty?," *IEEE Trans. Autom. Control*, vol. 47, no. 11, pp. 1865-1871, November 2002.
- [12] G. Bertotti, "Hysteresis in magnetism," *Academic Press*, May 20, 1998.
- [13] S. Mittal and C.H. Menq, "Hysteresis Compensation in Electromagnetic Actuators Through Preisach Model Inversion," *IEEE/ASME Transactions on Mechatronics*, vol. 5, no. 4, pp. 394-409, December 2000.
- [14] M.L. Hodgdon, "Application of a theory of ferromagnetic hysteresis," *IEEE Transactions on Magnetics*, vol. 24, no. 1, pp. 218-221, January 1988.
- [15] L. Li, "Linearizing magnetic bearing actuators by constant current sum, constant voltage sum, and constant flux sum," *IEEE Transactions on Magnetics*, vol. 35, no. 1, pp. 528-535, January 1999.
- [16] S.E. Zirka, Y.I. Moroz, P. Marketos, A.J. Moses, D.C. Jiles, and T. Matsuo, "Generalization of the classical method for calculating dynamic hysteresis loops in grain-oriented electrical steels," *IEEE Transactions on Magnetics*, vol. 44, no. 9, pp. 2113-2126, September 2008.
- [17] D.L. Trumper, S.M. Olson, and P.K. Subrahmanyam, "Linearizing control of magnetic suspension systems," *IEEE Trans. Contr. Syst. Technol.*, vol. 5, no. 4, July 1997.
- [18] E.P. Furlani, "Permanent magnetic and electromechanical devices," Academic press series in electromagnetism, Academic Press, 2001.
- [19] R.V. Iyer, and X. Tan, "Control of hysteretic systems through inverse compensation," *IEEE Control Syst. Mag.*, vol. 29, no. 1, pp. 83-99, Feb. 2009.
- [20] A. Katalenic, C.M.M. van Lierop and P.P.J. van den Bosch, "Smooth parametric hysteresis operator for control," *IFAC 18th World Congress*, Milano 2011.
- [21] A. Katalenic, J. de Boeij, C.M.M. van Lierop and P.P.J. van den Bosch, "Linearization of the reluctance force actuator based on the parametric hysteresis inverse and a 2D spline," *The Eighth International Symposium on Linear Drives for Industry Applications*, Eindhoven 2011.